SUPPLEMENTARY MATERIALS

Transcription regulation of the *Staphylococcus aureus* multidrug efflux operon *mepRA* by the MarR family repressor MepR

Ivan Birukou[1], Susan M. Seo[2], Bryan D. Schindler[2], Glenn W. Kaatz[2,3], Richard G. Brennan[1]*

[1] Department of Biochemistry, Duke University School of Medicine, Durham, North Carolina 27710, USA

[2] The John D. Dingell Department of Veterans Affairs Medical Center, Detroit, Michigan 48201, USA

[3] Department of Medicine, Division of Infectious Diseases, Wayne State University School of Medicine, Detroit, Michigan 48201, USA

*To whom correspondence should be addressed. Tel: (919) 684-9471; Fax: (919) 684-8885; Email: richard.brennan@duke.edu

Table S1. Thermodynamic parameters and oligodeoxynucleotide sequences for WT and mutated MepR proteins binding to the *mepR* and *mepA* operator sites*.

MepR variant	DNA	n	K_d, nM	ΔH, kcal/mol	ΔS, cal/(mol•deg)
WT	27 bp *mepR* site: 5'-TATTTAGTTAGACATCTAACGAAATGG-3'	1.92	36.6	8.73	63.3
WT	14 bp *mepR* site: 5'-GTTAGACATCTAAC-3'			No binding	
WT	18 bp *mepR* site: 5'-TAGTTAGACATCTAACGA-3'	0.52	2012.1	15.45	77.9
WT	27 bp *mepR* site with scrambled recognition helix binding region: 5'-TATTTACTATGTGTATCTAGGAAATGG-3'			No binding	
WT	27 bp *mepR* site with GC-rich wing binding sites: 5'-GCGGGCGTTAGACATCTAACGCCCGCC-3'	0.56	2036.7	16.78	82.3
WT	27 bp *mepR* site with flipped wing binding sites: 5'-ATAAATGTTAGACATCTAACGTTTAGG-3'	1.81	178.3	12.67	73.4
WT	26bp palindromized mepR site: 5'-TATTTAGTTAGATATCTAACTAAATA-3'	1.85	25.2	7.51	59.9
WT	26bp palindromized mutant mepR site: 5'-TATTTAG**A**TAGATATCTA**T**CTAAATA-3'	2.18	32.3	4.80	50.4
WT	26bp palindromized mutant mepR site: 5'-TATTTAGTT**T**GATATC**A**AACTAAATA-3'	2.04	94.3	9.00	62.3
WT	26bp palindromized mutant mepR site: 5'-TATTTAGT**A**AGATATCT**T**ACTAAATA-3'	2.02	76.9	6.66	54.9
WT	26bp palindromized mutant mepR site: 5'-TATTTAG**AAT**GATATC**ATT**CTAAATA-3'	2.29	10400.0	6.01	43.0
WT	26bp palindromized mutant mepR site: 5'-TATTTAGTTA**A**ATAT**T**TAACTAAATA-3'	1.91	8330.0	20.15	90.8

WT	46mer *mepA* operator: 5'-TATTATAGTTAGATATCTAATTGTTAGTAAGCTAATTATTGGAAAA-3'	3.87	41.7	7.42	58.6
WT	46mer *mepA* operator with 1st site intact, 2nd site scrambled: 5'-TATTATAGTTAGATATCTAATT**GTATTGAGATTACAACTTAGTAAT** -3'	2.17	71.9	4.47	47.7
WT	46mer *mepA* operator with 1st site scrambled, 2nd site intact: 5'-**TATGTCAGTAATTTATTCAAT**TGTTAGTAAGCTAATTATTGGAAAA -3'	2.32	3802.3	7.12	48.7
WT	26mer *mepA* operator, 2nd site only: 5'- CTAATTGTTAGTAAGCTAATTATTGG-3'	2.14	39.8	7.64	59.5
T63A	27 bp *mepR* site: 5'-TATTTAGTTAGACATCTAACGAAATGG-3'	2.06	14.6	6.60	58.0
H35A	27 bp *mepR* site: 5'-TATTTAGTTAGACATCTAACGAAATGG-3'	2.17	422.0	6.35	50.5
H14A	27 bp *mepR* site: 5'-TATTTAGTTAGACATCTAACGAAATGG-3'	1.94	380.2	8.29	57.2
R10S	27 bp *mepR* site: 5'-TATTTAGTTAGACATCTAACGAAATGG-3'	2.10	301.2	4.96	46.5

*n, stoichiometry of binding; n = 2 assumes that two protomers of MepR, which form a dimer, bind one duplex DNA, and is observed when MepR is titrated into DNA; n = 0.5 assumes one duplex DNA binds two protomers of MepR, which form a dimer, and is observed in reverse titration experiments, in which DNA is titrated into protein; n = 4 assumes 2 dimers of MepR (4 protomers total) bind a DNA duplex and is observed when MepR is titrated into wild type *mepA* operator DNA. K_d, the dissociation constant of the MepR-DNA complex. ΔH, enthalpy change of the reaction; ΔS, entropy change of the reaction. Inverted repeats are underlined, mutated sequences are shown in bold.

Table S2. Repression of chromosomal *mepR* and *mepA* expression by WT and mutant MepR proteins. All data are normalized to the activity of WT MepR.

MepR derivative	Repressor activity, mean ± standard deviation	
	mepR operator	***mepA operator***
WT	100.0	100.0
T63A	54.0 ± 11.1	95.0 ± 2.9
N66A	94.2 ± 8.6	99.6 ± 0.1
R69A	99.2 ± 7.1	99.1 ± 1.9
N70A	76.6 ± 9.2	99.7 ± 1.2
D85S	24.1 ± 8.3	30.1 ± 7.7
R87A	19.4 ± 5.3	0

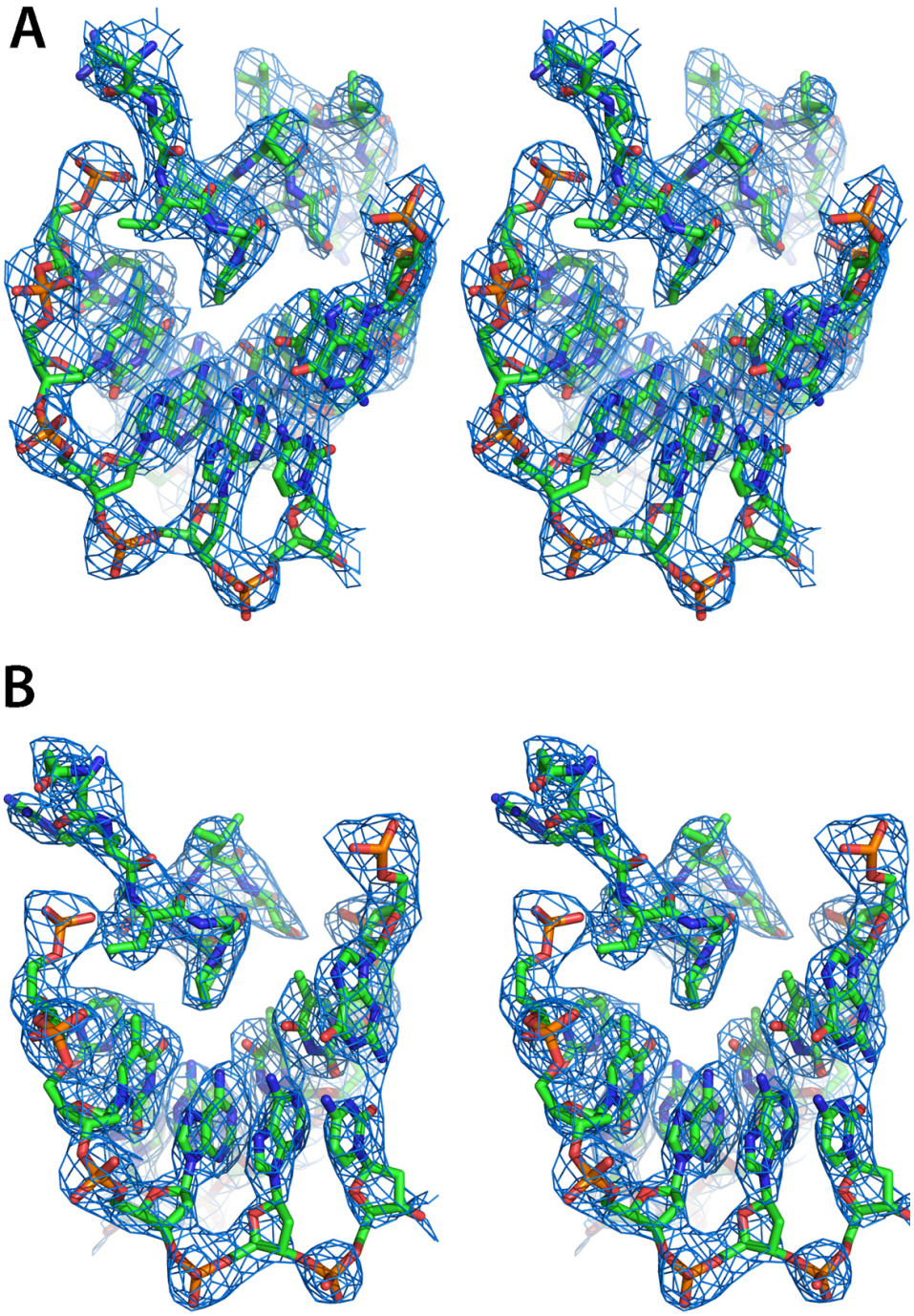

Figure S1. Cross-eyed stereo views of the 2Fo-Fc omit maps of the N-terminal portion of the recognition helix, which includes residues 58-66, and the bases of the major groove of the GTTAG signature motif. **(A)** Map from the omitted triclinic crystal form. **(B)** Map from the omitted trigonal crystal form. Maps are contoured at 1σ.

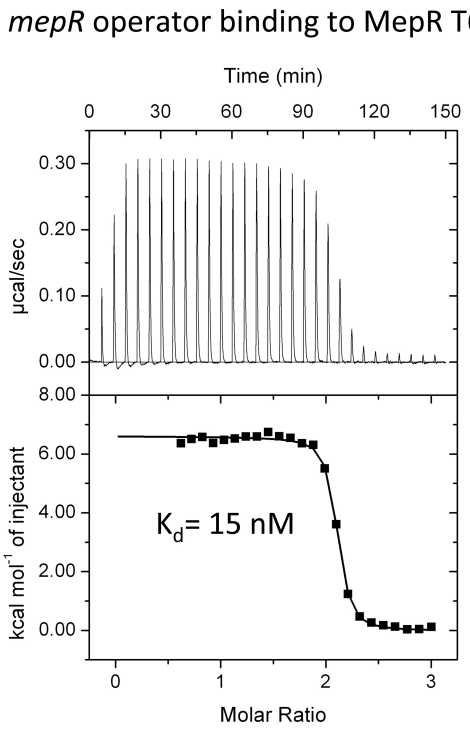

Figure S2. Representative thermogram and isotherm of MepR(T63A) binding to the *mepR* operator. MepR (140 µM) was injected into dsDNA solution (10 µM). The stoichiometry is 2, which corresponds to 1 dimer of MepR binding to a dsDNA. The fitted thermodynamic parameters are provided in Table S1.

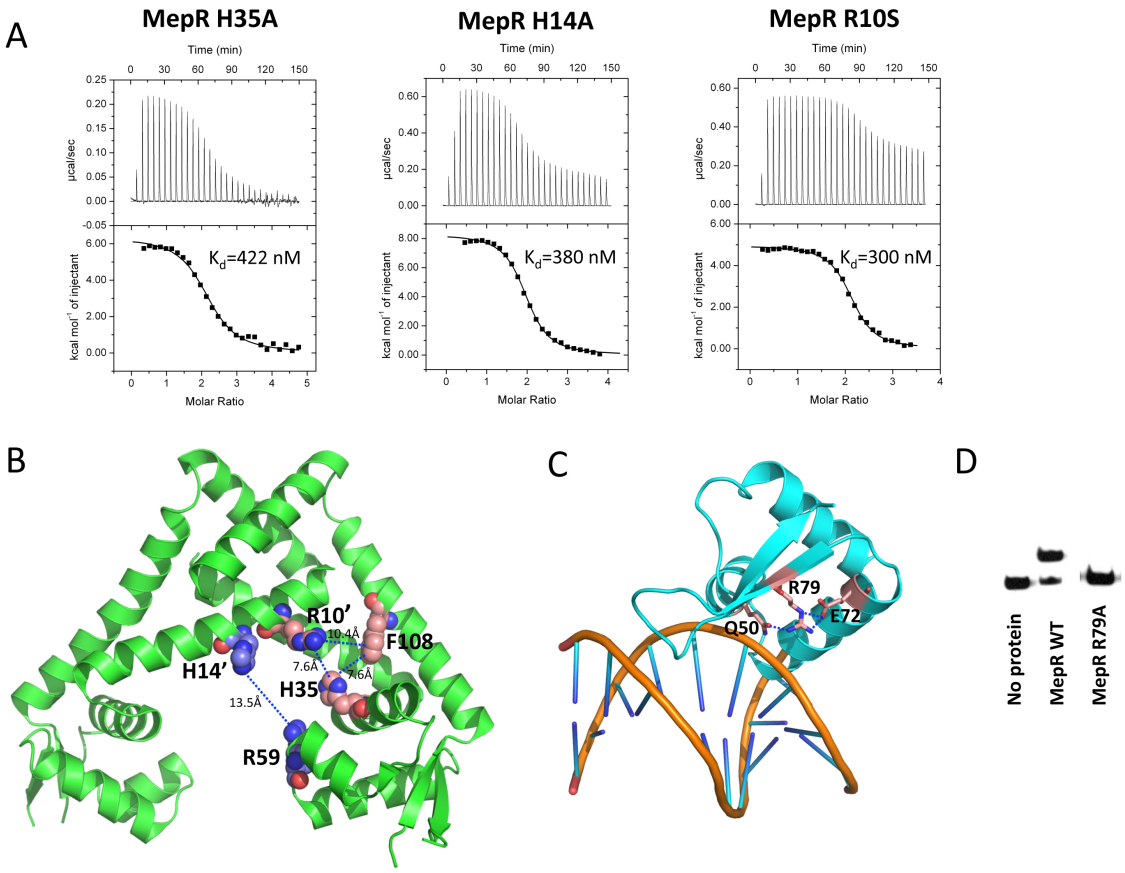

Figure S3. Inter and intramolecular protein-protein contacts in MepR contribute to high affinity DNA binding. **(A)** Binding of the MepR single mutants, H35A, H14A and R10S, to the 27 bp *mepR* operator DNA. In all three experiments, MepR (111 µM, 184 µM, and 180 µM, respectively) was injected into dsDNA (5 µM, 9 µM, and 10 µM, respectively). The stoichiometry of binding is n ~ 2 and corresponds to 1 dimer of MepR binding to a dsDNA. The fitted thermodynamic parameters are provided in Table S1. **(B)** The positions of residues H14, R10, H35, R59, and F108 in the apoMepR structure. The residues are shown as spheres, carbon atoms in the H14':R59 pair are light blue, carbon atoms of the R10':H35:F108 triad are coloured beige, oxygens are coloured red, and nitrogens are coloured blue. **(C)** Electrostatic interactions between residues Q50, R79, and E72 in the MepR-DNA complex. The residues are shown as sticks, carbons are coloured beige, oxygens red, and nitrogens, blue. The distance between Q50 and R79 is 3.5 Å, and between R79 and E72 ~3 Å. **(D)** MepR(R79A) does not bind to the *mepR* operator DNA as analysed by an electrophoretic mobility shift assay. 50 ng of wild type MepR or MepR(R79A) was incubated with 167 bp biotin-labelled oligodeoxynucleotide containing *mepR* operator DNA, generated by PCR.

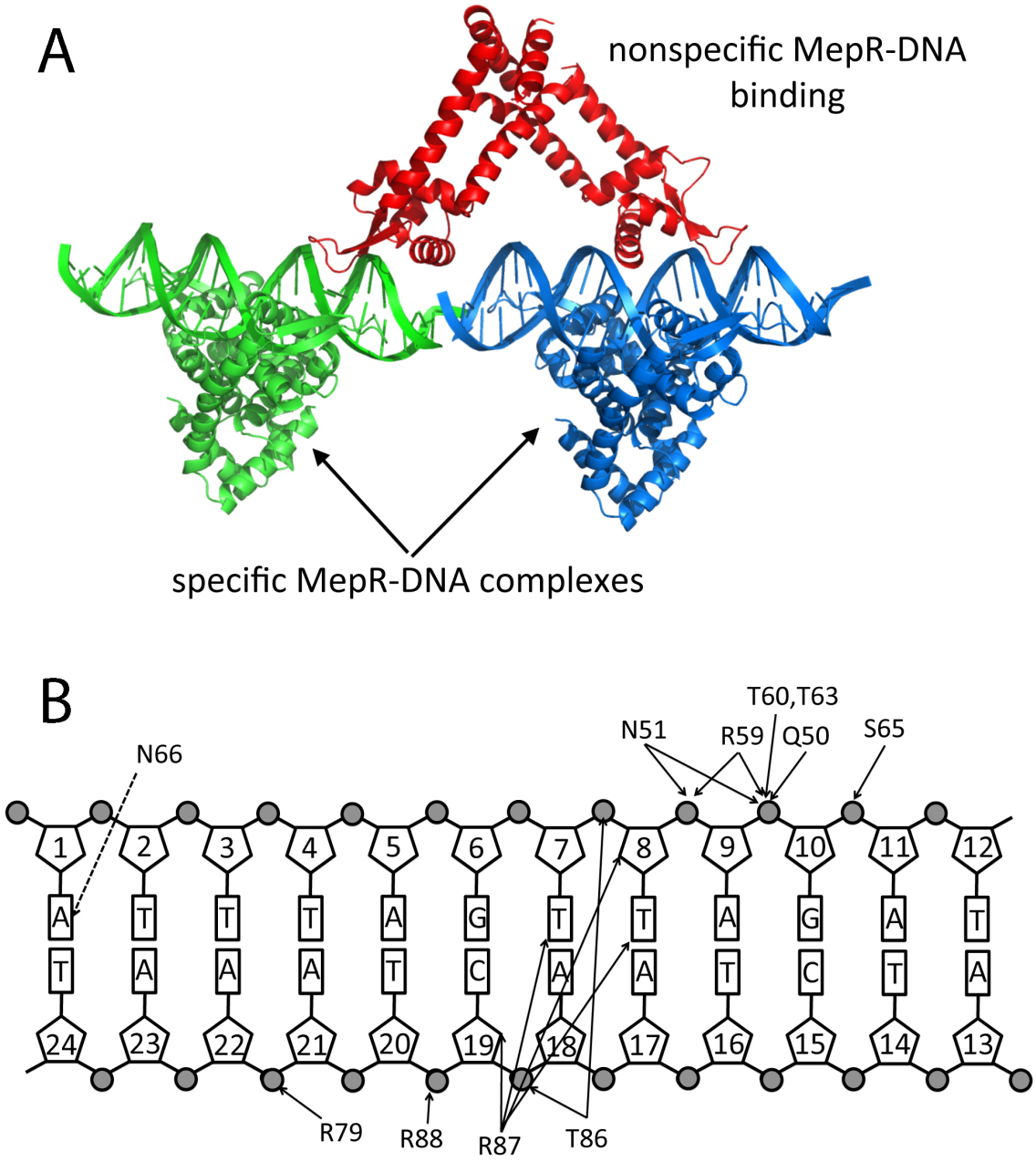

Figure S4. Nonspecific MepR-DNA interaction. **(A)** The MepR dimer, interacting nonspecifically with the two MepR-DNA complexes (green and blue) is shown as a red ribbon. **(B)** Schematic representation of protein-DNA interactions in nonspecific MepR-DNA complex. Solid arrows indicate electrostatic (hydrogen bonds or salt bridges) interactions, dashed arrows indicate van der Waals contacts. The contacts from both DNA binding domains to different oligodeoxynucleotides are combined on one DNA scheme.

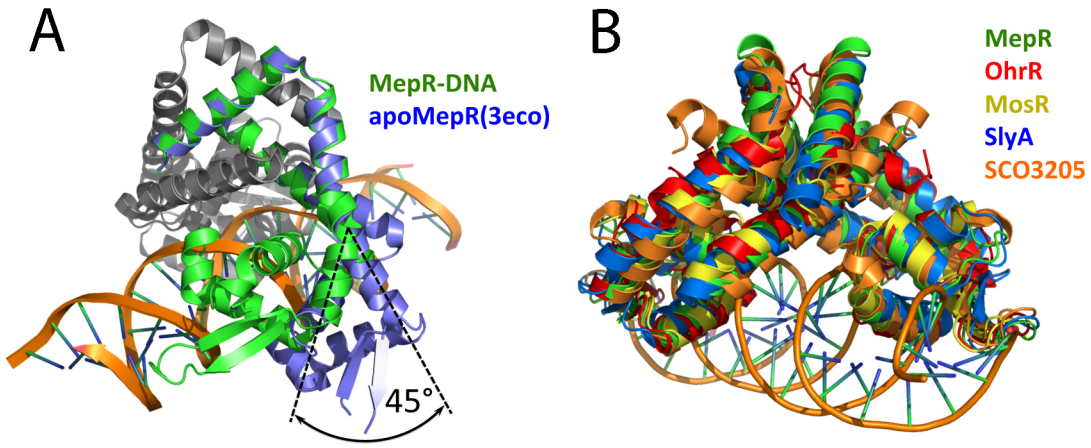

Figure S5. **(A)** Comparison of the DNA-bound MepR structure to that of an apoMepR, "induced" structure (PDB accession code 3eco). The dimerization domains were aligned. Only one subunit of each structure is colored. Dashed lines indicate the ~45° rotation of the wHTH domain needed for specific DNA binding. **(B)** Structural alignment of the MepR in complex with DNA with the DNA-bound dimers of *B. subtilis* OhrR (PDB accession code 1z9c), *S. coelicolor* SCO3205 (PDB accession code 3zpl), *M. tuberculosis* MosR (PDB accession code 4fx4), and *S. enterica* SlyA (PDB accession code 3q5f). Only the *mepR* operator DNA is shown for clarity.

Nonspecific MepR-DNA complex

In addition to the three independent MepR-DNA complexes that are seen in the asymmetric unit of the trigonal crystals, an additional MepR dimer is bound to DNA. However, unlike the specific complexes, this fourth dimer interacts with two different DNA molecules acting as a nonspecific tether (Figure S4A). Further, the protein-DNA interactions are different for each subunit of this dimer whereby the wHTH motif of one subunit inserts its recognition helix into the central major groove of the *mep*R operator DNA and not the major groove encompassing the signature sequence, whilst the second subunit does not engage the major groove *per se*. Further, the recognition helix of the former subunit does not insert deeply into the major groove and hence, only very weak van der Waals contacts are found between residues 60 through 63 and the bases. There is, however, a number of nonspecific electrostatic contacts that stabilize the helix-turn-helix motif-DNA interaction. For example, the phosphate group of A_9 forms a salt bridge with the side chain of residue Arg59, and the phosphate moiety of G_{10} interacts with the side chains of residues Arg59, Thr60 and Thr63. On the complimentary strand, the phosphate group of A_9 interacts with Asn51, the phosphate group of G_{10} - with residues Gln50 and Asn51, and Ser65 donates a hydrogen bond to the phosphate group of A_{11}. Additionally, the positive dipole of the N-terminus of α3 is directed towards the negatively charged sugar-phosphate backbone. Interestingly, a network of electrostatic interactions between the side chains of the recognition helix of the nonspecific MepR dimer and that of the specific MepR is observed. Specifically, the Arg69:Arg73*:Arg69* triplet (where the asterisk indicates the amino acid residues from the specifically bound MepR), are involved in π-π stacking interactions, analogous to those observed for Arg10':His35:Phe108 triad. In addition, residue Asn66 interacts with both Arg69* and Arg73*. This network likely contributes to the stability of the nonspecific MepR-DNA complex.

The interaction between the recognition helix of the wHTH domain of the second subunit and DNA is unusual (Figure S4A). In this interaction, the α4

recognition helix is inserted into the major groove created by the ends of two independent DNA duplexes that stack to form pseudo-continuous double helix. With exception of residue Asn66, the side chain of which is located ~4 Å from the N7 atom of A_1, all residues of the recognition helix are too far from either the bases or the sugar-phosphate backbone to form strong electrostatic or van der Waals interactions. Again, the positively charged dipole of α3 and the negatively charged sugar-phosphate backbone contribute to binding. In general, almost all interactions observed in the nonspecific complex are analogous to those seen in the specific MepR-DNA structure (Figures 3, S4B). However, the nonspecific MepR-DNA complex lacks numerous protein-DNA backbone interactions, and more importantly, the van der Waals contacts between the recognition helices and major grooves, which are crucial for the recognition of high affinity sites.

As observed in the specific MepR-DNA complexes, the wing motif of the nonspecifically bound MepR inserts into the neighboring minor groove, where the side chain of residue Arg87 donates a hydrogen bond to the O2 atom of T_8 and ribosyl oxygens of T_8 and C_{19}. Furthermore, wing residue Thr86 interacts with the phosphate group of C_{19}. The wing of the second subunit interacts with the minor groove of a neighboring DNA duplex. In a similar manner, the side chain of residue Arg87 donates hydrogen bonds to the O2 atoms of bases T_7 and T_8, as well as to the ribosyl oxygen of T_8. Residue Thr86 interacts with the phosphate of T_8, whilst residues Arg79 and Arg88 establish salt bridges with the phosphates of A_{22} and T_{20} of the complementary strand. Overall, the wing-mediated interactions in nonspecific MepR-DNA complex are essentially identical to the wing-minor groove interactions observed in the specific MepR-DNA complex, except that the DNA sequence is shifted by four base pairs: in the specific complex, the guanidinium group of residue Arg87 interacts with T_4, whereas in the nonspecific complex the Arg87 side chain reads thymines 7 and 8, which belong to GTTAG signature sequence (Figures 3, S4B).

Interestingly, the dimerization domain of the nonspecifically bound MepR dimer is significantly disordered and due to poor electron density, residues 115 to

124 could not be built. Regardless, the overall configuration of the dimer is discernable and is distinct from the specific DNA-binding conformation of MepR. Indeed, the distance between the centers of the recognition helices is ~42 Å, and the orientations of recognition helices are substantially different from those of MepR in complex with DNA. As a result, the alignment of the dimer from the MepR-DNA complex with the nonspecifically bound MepR dimer produces a striking RMSD of 6.5 Å. Further, the conformation of the nonspecific MepR dimer is also distinct from the apoMepR (PDB accession code 3eco) dimer (RMSD = 4.9 Å), which again demonstrates the great flexibility and adaptability of the MarR family members. We propose that this MepR-DNA complex provides fortuitous insight into one of the nonspecific DNA binding modes of MepR and, potentially other MarR family members.